다중 파괴기준의 소성모델을 이용한 철근콘크리트부재의 비선형 해석

Nonlinear Analysis of Reinforced Concrete Members using Plasticity with Multiple Failure Criteria

박홍근*
Park, Hong Gun

요 약

콘크리트는 압축압밀과 인장균열파괴의 두개의 서로 다른 파괴양상을 나타낸다. 따라서, 다차원의 압밀과 인장균열을 포함하는 콘크리트의 비선형해석을 위하여 두개의 다른 파괴기준을 사용하는 콘크리트 재료모델이 사용되어야 한다. 본 연구에서 사용하는 콘크리트 모델은 소성이론에 기초한 것으로 압축압밀과 인장균열에 대한 다중파괴이론을 사용하고 있다. 인장균열거동에 대해 두개의 다른 재료모델이 사용되고 있는데, 이상화된 균열방향에 따라 분류되는 회전균열소성모델과 정지균열소성모델이 사용되고 있다. 본 연구에서는 콘크리트의 비선형거동이 plane stress 문제에 대하여 단순화된다. 이 재료모델은 유한요소해석에 사용되며 그 결과는 몇 개의 철근콘크리트부재 실험과 비교된다. 회전균열소성모델과 정지균열소성모델의 장단점이 비교된다.

Abstract

Concrete has two different failure mechanisms : compressive crushing and tensile cracking. Concrete models should use the two different failure criteria to analyze the inelastic behavior of concrete including multiaxial crushing and tensile cracking. Concrete models used in this study are based on plasticity with multiple failure criteria of compressive crushing and tensile cracking. For tensile cracking behavior, two different plasticity models are investigated. These are rotating-crack and fixed-crack plasticity models, classified according to idealization of crack orientations. The material models simplify inelastic behavior of concrete for plane stress problems. The material models are used for the finite element anlaysis. Analytical results are compared with several experiments of reinforced concrete member. The advantages and disadvantages of rotating-crack and fixed-crack plasticity models are discussed.

Keywords : reinforced concrete, multiple failure criteria, rotating-crack and fixed-crack platicity, plane stress, and finite element analysis

* 정회원, 미국 오스틴 소재 텍사스대학교 연구원, 공학박사

• 본 논문에 대한 토의를 1995년 12월 31일까지 학회로 보내 주시면 1996년 2월호에 토의회답을 게재하겠습니다.

1. Introduction

Concrete failure is characterized by compressive crushing and tensile cracking. Crushing failure induces a relatively wide-spread damage which has no specific directionality. On the other hand, cracking has the characteristics of directionality and localization. Crushing and cracking can also occur simultaneously in tension-compression. Accordingly, the different types of concrete failure should be addressed in the analysis of plain and reinforced concrete structures. In concrete plasticity, two different failure criteria for crushing and cracking are required.

Due to the complexity of tensile cracking, it is difficult to idealize the directionality of tensile crackes though the material models of plain and reinforced concrete use idealized crack orientations. Concrete models that are frequently used in compurter analysis of plain or reinforced concrete structures are orthotropic axes models using equivalent uniaxial stress-strain curves(see Park[7]). Though the orthotropic axes models are fairly easy to use in analysis because of the simplicity, they have difficulty in producing reliable results in multiaxial compression. The orthotropic axes models are classified into fixed-crack and rotating-crack models according to the idealization of crack orientations. The idealization of crack orientations is also applicable to the tensile failure criterion of plasticity models.

Plasticity theory usually used for multiaxial compression are applicable for tensile cracking. If cracking failure surfaces are defined with principal stresses, this plasticity model can not define specific crack orientations(see Feenstra and Borst[4]). Instead, this plasticity model, referred to as rotating-crack plasticity, can simulate the rotation of principal stress axes due to the progressive cracking process. The rotating-crack plasticity is analogous to the rotating-crack model of the orthotropic axes approach.

The program ABAQUS[1] uses a different cracking failure criterion. Tensile crack orientations are fixed as soon as the initial cracks develop. The tensile behavior after cracking is defined in the fixed crack orientations. This cracking plasticity is referred to as fixed-crack plasticity.

It would be worthwhile to compare fixed-crack and roating-crack plasticity models. However, such comparison has not been reported. For the orthotropic axes model, several examples of the comparison between fixed-crack and rotating-crack models have been published. In the orthotropic axes model, however, the idealization of the orthotropic axes controls compressive as well as tensile behavior. Accordingly, it is difficult to compare the effectiveness of the two crack models for tensile cracking. For example, rotating-crack models show better agreement with heavily reinforced members whose failure occurs due to crushing after extensive cracking. Fixed-crack models overestimate the ultimate strengths. This is because the equivalent uniaxial stress-strain relation in the idealized fixed crack orientation overestimates the compressive strength of concrete.

In the plasticity models with multiple failure criteria, the tensile failure criterion is independent of compressive crushing, and it is possible to compare the effectiveness of the rotating and the fixed crack plasticity for tensile behavior. Such comparison is the emphasis of this paper.

2. Material Model

The plasticity material model uses isotropic hardening and multiple failure criteria for compressive crushing and tensile cracking. In compression-dominant circumstances, the crushing failure surface activates earlier causing the inelastic behavior due to crushing to dominate over that due to cracking. The opposite is true in tension-dominant circumstances.

The material model simplifies the actual concrete behavior for plane stress problems though it can be used for vairous load conditions. As a crushing failure criterion, von Mises criterion is used. The failure criterion with associative flow tends to oversimplify the actual concrete behavior. But, it is simple for application and relatively accurate for plane stress problem which is less affected by excessive hydrostatic pressure and inelastic volumetric strain[4,5]. The material model uses rotating-crack and fixed-crack plasticity for cracking behavior.

In fixed-crack plasticity, when the tensile stress in a principal incremental strain axis approaches the cracking stress, the cracking failure criterion activates in that axis. Also, the shear stiffness related to the axis decrease after the tensile cracking. Accordingly, the orthotropic characteristics of cracked concrete are established in the principal incremental strain axes after cracking. Under further loading, the orthotropic axes is fixed to the initial crack orientation. The material behavior of the cracked concrete is defined in the orthotropic axes. Also, another failure surface for cracking is examined normal to the initial crack direction. As a result, as many as three failure surfaces for crushing and cracking in two orthogonal axes may activate simultaneously in plane stress.

In rotating-crack plasticity, the orthotropic axes continuously rotate to the principal stress axes even after cracking occurs. The maximum tensile stress in the principal tensile axis depends on the cracking failure surface function. Since the principal tensile stress axis represents the crack orientation, only one crack direction exists without additional crack directions. However, multiple crack directions are not likely to exist under monotonic loading. In plane stress condition, as many as two failure surfaces may activate simultaneously in the rotating-crack plasticity.

3. Failure Criteria for Crushing and Cracking

The von Mises criterion is

$$f_1=\sigma_{el}-\bar{\sigma}_1(\varepsilon_{pl})=\sqrt{\frac{3}{2}\,\underline{s}\cdot\underline{s}}\quad-\bar{\sigma}_1(\varepsilon_{pl}) \qquad (1)$$

where σ_{el} is the effective stress and $\bar{\sigma}_1$ is the failure surface function of equivalent plastic strain, ε_{pl}. The subscript "1" indicates compressive crushing. The equivalent plastic strain, ε_{pl}, has the following relation with the failure criterion.

For the vector of plastic strain rate, an associative flow is used.

$$\dot{\varepsilon}_{pl}=\dot{\lambda}_1\left(\frac{\partial f_1}{\partial \underline{\sigma}}\right)=\dot{\lambda}_1\,\underline{a}_1 \qquad (2)$$

where $\dot{\lambda}_1$ is the plastic strain rate multiplier. The equivalent plastic strain rate is defined by the scalar product of the vector of plastic strain rate.

$$\dot{\varepsilon}_{pl}=\sqrt{\frac{2}{3}(\dot{\underline{\varepsilon}}_{pl}\cdot\dot{\underline{\varepsilon}}_{pl})}=C_1\dot{\lambda}_1 \qquad (3)$$

The equivalent plastic strain in Eq. 1 is

accumulated from the equivalent plastic strain rate.

$$\varepsilon_{p1} = \int \dot{\varepsilon}_{p1} \tag{4}$$

In Fig. 1, the failure surface $\bar{\sigma}_1$ is defined by the function of the equivalent plastic strain ε_{p1}.

The failure criterion of tensile cracking is

$$f_2 = \sigma_{e2} - \bar{\sigma}_2(\varepsilon_{p2}) \tag{5}$$

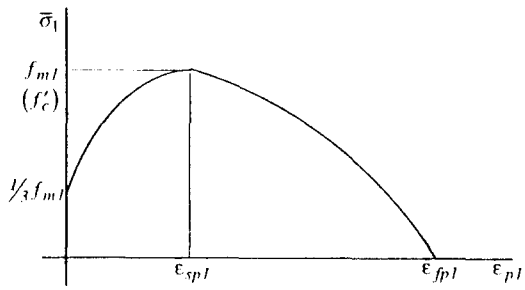

$$\varepsilon_{sp1} \geq \varepsilon_{p1} \qquad \bar{\sigma}_1 = \frac{f_{m1}}{3}\left(1 + 4\frac{\varepsilon_{p1}}{\varepsilon_{sp1}} - 2\frac{\varepsilon_{p1}^2}{\varepsilon_{sp1}^2}\right)$$

$$\varepsilon_{sp1} < \varepsilon_{p1} \leq \varepsilon_{fp1} \qquad \bar{\sigma}_1 = f_{m1}\left(1 - \frac{(\varepsilon_{p1} - \varepsilon_{sp1})^2}{(\varepsilon_{fp1} - \varepsilon_{sp1})^2}\right)$$

Fig. 1 Failure surface function used for crushing failure criterion

For the fixed-crack plasticity, the effective stress, σ_{e2}, is the tensile stress component either in current principal incremental strain axes before cracking or in the fixed orthotropic axis after cracking. For the rotating-crack plasticity, the effective stress is current principal tensile stress.

The equivalent plastic strain rate is

$$\dot{\varepsilon}_{p2} = \dot{\lambda}_2 \left(\frac{\partial f_2}{\partial \underline{\sigma}}\right) = \dot{\lambda}_2 \underline{a}_2 \tag{6}$$

where the subscript "2" indicates the cracking failure criterion.

In Fig. 2, the cracking failure surface, $\bar{\sigma}_2$, is

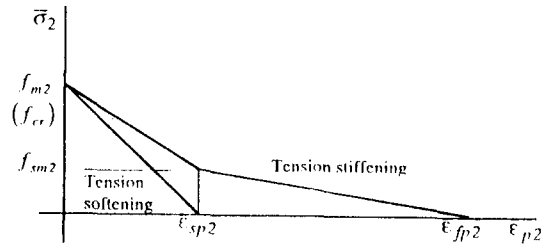

Fig. 2 Failure surface function used for cracking failure criterion

defined by the function of the equivalent plastic strain, ε_{p2}. For the post-cracking behavior, the tensile failure surface considers tension softening due to cracking and tension stiffening due to the interaction between cracked concrete and reinforcement. In this figure,

$$f_{sm2} = 40\rho_e f_{m2} \leq 0.4 f_{m2} \tag{7}$$

where $\rho_e = \Sigma\rho_i \cos^2\theta_i$, and θ_i is the angle between the orientation of the initial crack and a reinforcing steel layer.

$$\varepsilon_{fp2} = \frac{1}{\rho_e}\Sigma(\varepsilon_{syi}\rho_i \cos^2\theta_i) \tag{8}$$

where ε_{syi} is the yield strain of corresponding reinforcing steel layer.

$$\varepsilon_{sp2} = \frac{2G_t}{h f_{m2}} \tag{9}$$

where G_t is the fracture energy of tensile

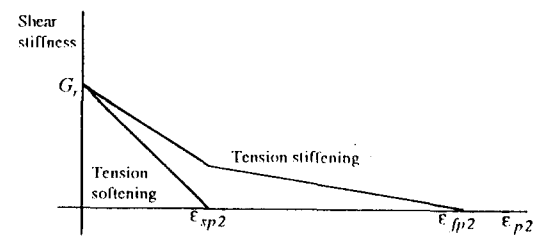

Fig. 3 Reduced shear stiffness due to cracking in fixed-crack plasticity

cracking, and h is the effective length corresponding to a Gauss point.

As shown in Fig. 3, the shear stiffness is significantly reduced due to tensile cracking in the fixed-crack plasticity.

4. Integration of Flow Rules

As a scheme to return the stresses to corresponding failure surface following an initially predicted stresses, a simple backward-Euler scheme is used(see Crisfield[3]). In inelastic behavior, the failure criteria are not satisfied with the initial elastic predictor. Then, a first-order Taylor expansion of the failure criteria gives

$$f_i^1 = f_i^0 + \left(\frac{\partial f_i^0}{\partial \underline{\sigma}^0}\right)^T \Delta\underline{\sigma}^0 + \left(\frac{\partial f_i^0}{\partial \underline{\varepsilon}_{pl}^0}\right) \Delta\underline{\varepsilon}_{pl}^0 = 0 \text{ or}$$

$$f_i^1 = f_i^0 + \underline{a}_i^T \Delta\underline{\sigma}^0 - H_i C_i \Delta\lambda_i^0 = 0 \qquad i=1, 2, 3 \quad (10)$$

where the superscript "0" indicates current iteration. As mentioned before, as many as three failure surfaces can activate simultaneously. The stress increments in current iteration are

$$\Delta\underline{\sigma}^0 = \underline{D}(\Delta\underline{\varepsilon}_e^0) = \underline{D}(\Delta\underline{\varepsilon}^0 - \Delta\underline{\varepsilon}_p^0)$$
$$= \underline{D}(\Delta\underline{\varepsilon}^0 - \Sigma\Delta\underline{\varepsilon}_{pl}^0) = \underline{D}(\Delta\underline{\varepsilon}^0 - \Sigma\underline{a}_i^0 \Delta\lambda_i^0) \quad (11)$$

In the finite element analysis, it is needed to obtain total stress increments corresponding to given total strain increments. Accordingly, set $\Delta\underline{\varepsilon}^0 = \underline{0}$ after the initial elastic predictor.

From Equations 10 and 11, the plastic strain rate multiplier can be obtained :

$$\underline{A} \cdot \Delta\underline{\lambda}^0 = \underline{F}^0 \quad (12)$$

where $\Delta\underline{\lambda}^0 = \langle\, \Delta\lambda_1^0\ \Delta\lambda_2^0\ \Delta\lambda_3^0 \,\rangle^T$

$\underline{F}^0 = \langle\, f_1^0\ f_2^0\ f_3^0 \,\rangle^T$, and

$A_{ij} = \underline{a}_i^T \underline{D} \underline{a}_j + H_i\, C_i\, \delta_{ij}$

The updated stresses and equivalent plastic strains are

$$\underline{\sigma}^1 = \underline{\sigma}^0 - \Sigma(\underline{D} \cdot \Delta\underline{\varepsilon}_{pl}^0) = \underline{\sigma}^0 - \Sigma(\underline{D} \cdot \underline{a}_i^0\, \Delta\lambda_i^0), \text{ and}$$
$$\varepsilon_{pl}^1 = \varepsilon_{pl}^0 + C_i\, \Delta\lambda_i^0 \quad (13)$$

In Eq. 13, the initially predicted stresses are relaxed by the backward-Euler procedure. If the updated failure criteria with new stress components, Eq. 10, are not sufficiently small, this relaxation procedure is applied again.

The backward-Euler procedure used for the integration should be modified for multiple plasticity. Sometimes, the backward-Euler procedure does not accomplish convergence to failure surfaces with a reasonable number of iterations. This is becasue Eq. 12 yields unexpectedly large or negative plastic strain rate multipliers. This indicates that the given strain increments are too large for the integration. The given strain increments can then be divided into small steps, and iterations are needed each step up to the given strain increments.

5. Consistent Tangent Stiffness Matrix

For fast and stable convergence in nonlinear calculation of plasticity, the tangent stiffness matrix needs to be consistent with the backward-Euler procedure. Differentiation of Eq. 11 gives

$$\dot{\underline{\sigma}} = \underline{D}\,\dot{\underline{\varepsilon}} - \Sigma(\dot{\lambda}_i \underline{D} \cdot \underline{a}_i) - \Sigma(\Delta\lambda_i \underline{D} \cdot (\frac{\partial \underline{a}_i}{\partial \underline{\sigma}})\dot{\underline{\sigma}}) \text{ or} \quad (14)$$

$$\dot{\underline{\sigma}} = (\underline{I} + \Sigma(\Delta\lambda_i \underline{D} \cdot (\frac{\partial \underline{a}_i}{\partial \underline{\sigma}})))^{-1} \underline{D}(\dot{\underline{\varepsilon}} - \Sigma(\dot{\lambda}_i \underline{a}_i))$$
$$= \underline{R}(\dot{\underline{\varepsilon}} - \Sigma\dot{\lambda}_i \underline{a}_i)) \quad (15)$$

To remain on the failure surface, the expansion in Eq. 10 should disappear.

$$\dot{f}_i=(\frac{\partial f_i}{\partial \underline{\sigma}})^T \dot{\underline{\sigma}}+(\frac{\partial f_i}{\partial \varepsilon_{pi}}) \dot{\varepsilon}_{pi} = 0 \text{ or}$$

$$\dot{f}_i=\underline{a}_i^T \dot{\underline{\sigma}}-H_i C_i \dot{\lambda}_i = 0 \quad i=1, 2, 3 \qquad (16)$$

Using Equations 15 and 16,

$$\underline{B} \cdot \dot{\underline{\lambda}} = \underline{a}^T \cdot \underline{R} \dot{\underline{\varepsilon}} \qquad (17)$$

where $B_{ij}=\underline{a}_i^T \underline{R} \underline{a}_j + H_i C_i \delta_{ij}$ and $\underline{a}^T=\begin{bmatrix} \underline{a}_1^T \\ \underline{a}_2^T \\ \underline{a}_3^T \end{bmatrix}$

From Equations 17 and 15, the consistent tangent matrix can be derived :

$$\underline{D}_t=(\underline{R}-\underline{R}\ \underline{a}\ \underline{B}^{-1}\ \underline{a}^T\ \underline{R}^T) \qquad (18)$$

Implementation in Finite Element Method

The developed material models are used for finite element analysis. Reinforced concrete members are idealized by 4-node isoparametric elements. The bilinear kinematic hardening is used for the material model of reinforcing steel. The reinforcing steel can be used as either isoparametric elements with smeared properties or discrete line elements. As nonlinear computational scheme, a simplified displacement control method is used(see Ramm[8]). As mentioned in Ref. 6, the displacement control method produces better convergence rates than the arc-length method.

6. Application of Material Model

The concrete plasticity models are verified for a reinforced concrete beam and reinforced concrete masonry shear walls.

6.1 Reinforced Concrete Beam Tests(Bresler and Scordelis)

Bresler and Scordelis[2] investigated the shear capacity of a series of beam specimens. The properties and the analytical model of their Beam A-1 are shown in Fig. 4. The ratio of shear span to beam depth is 3.26. This beam has heavy longitudinal reinforcement at the bottom, so that inelastic flexural deformation due to yielding of reinforcing steel is prevented. On the other hand, the low reinforcement ratio of the vertical bars invites extensive diagonal tension cracking. The beam fails due to compressive crushing in the top middle of the beam. The heavy reinforcement in tension and diagonal tension cracking induce the shear-compression failure.

As shown in Fig. 5, the analytical result of the rotating-crack plasticity agrees well with

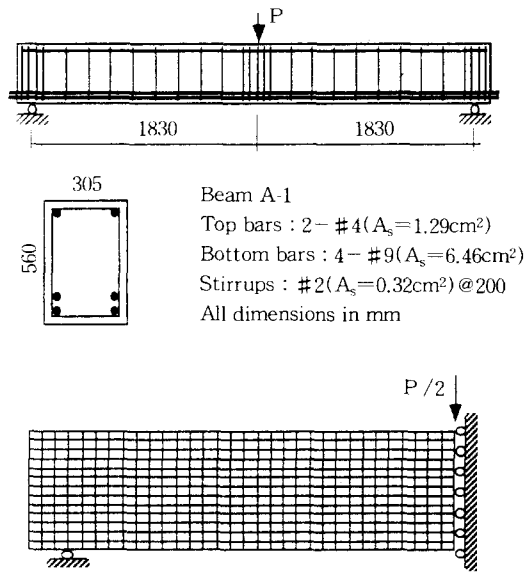

416 four-node rectangular elements and 64 two-node line elements Analytical half-beam model

Fig. 4 Reinforced concrete beam tested by Bresler and Scordelis

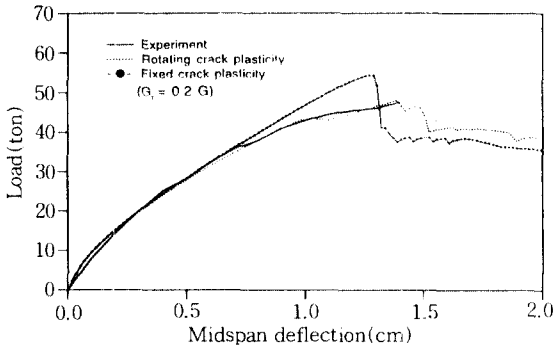

Fig. 5 Comparison between analyses and experiment of reinforced concrete beam(Bresler and Scordelis)

the experiment up to the maximum load capacity of the beam. On the other hand, the fixed-crack plasticity overestimates the maximum load capacity. The analysis with the reduced shear stiffness, G_r=0.1G(not shown in the figure) produces almost the same results as that with G_r=0.2G. This indicates that the idealized fixed crack directions significantly affect the analytical result rather than the reduced shear stiffness. The analyses also show sudden decrease of load capacity which indicates the brittle failure without much inelastic deformation.

The analyses have difficulty in numerical calculation at the sudden decrease of load capacity. As mentioned in Ref. 6, the crushing failure induces the change of the load-transfer mechanism and a sudden decrease of the load capacity. For the plasticity models which are incremental formulations, small variations of stress-strain relations are required during nonlinear analysis. However, the sudden decrease of the load capacity induces considerable variations of stress-strain relations across the member.

6.2 Reinforced Concrete Masonry Wall Tests (Shing et al.)

The plasticity models are applied for the reinforced concrete masonry shear walls tested by Shing et al.(see de la Rovere[9]) Walls 7, 10 and 12 are analyzed here. As shown in Fig. 6, the shear walls have a rigid base and a top slab. They are subjected to uniformly distributed vertical loads and a concentrated cyclic horizontal load at the top slab. The shear walls are reinforced by uniformly

Table 1 Loading conditions and material properties of shear walls tested by Shing et al.

Wall No.	Masonry σ_m' kg/cm²	Horizontal Steel		Vertical Steel		Axial load ton
		ρ_x %	f_{xy} kg/cm²	ρ_y %	f_{yy} kg/cm²	
7	205.1	0.14	3990	0.74	4925	18.2
10	225.5	0.14	3990	0.38	4433	18.2
12	225.5	0.24	4644	0.38	4433	18.2

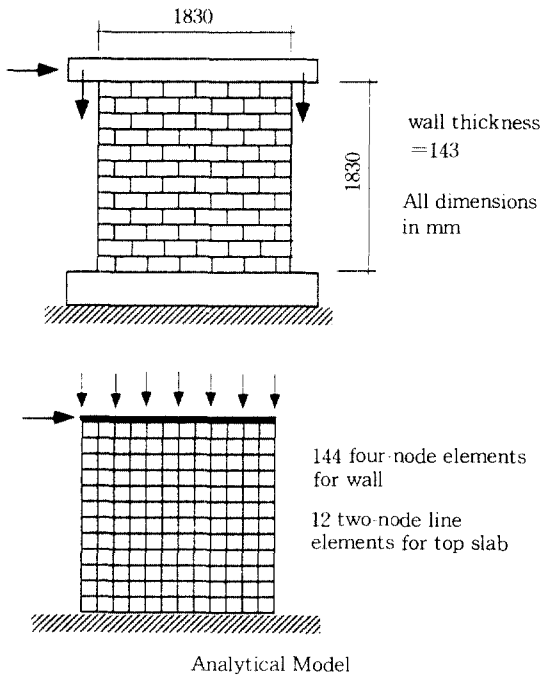

Fig. 6 Reinforced concrete masonry wall tested by Shing et al.

distributed vertical and horizontal steel layers. The loading conditions and the properties of materials are shown in Table 1. The analytical model is shown in Fig. 6.

Figures 7-9 show the envelopes of the cyclic load-deflection curves of Walls 7, 10 and 12. Walls 10 and 12, with similar horizontal and vertical reinforcement ratios, have a maximum horizontal load capacity of 30 tons, which gradually decreases with increasing displacement. Wall 12, with more horizontal reinforcement, shows more ductile behavior than Wall 10. Wall 7, with heavy vertical reinforcement, has a large shear capacity. However, due to the relatively light horizontal reinforcement, compression crushing occurs suddenly just after the maximum horizontal load.

In Figures 7-9, the analytical load-deflection curves under monotonic loading are compared with the envelopes of the experimental cyclic load-deflection curves. The rotating-crack plasticity produces better agreement with the maximum load of the experiments. The fixed-crack plasticity with G_r=0.2G overestimates the maximum loads. Neither crack plasticity follows the ductile behavior of Walls 10 and 12 and the sudden decrease of the load capacity of Wall 7.

Analytically, the rotating-crack plasticity is more stable in convergence than the fixed-crack plasticity. In the fixed-crack plasticity, the sudden decrease of the shear stiffness due to tensile cracking causes difficulty in numerical calculation.

7. Conclusion

Crushing and cracking can occur simultaneously in reinforced concrete. Crushing failure of cracked concrete is common in reinforced concrete members. Accordingly, the

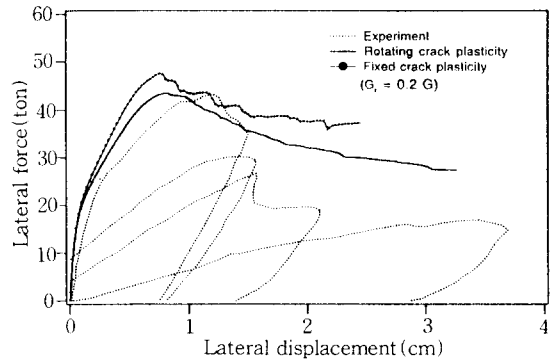

Fig. 7 Comparison between analyses and experiment for Wall 7

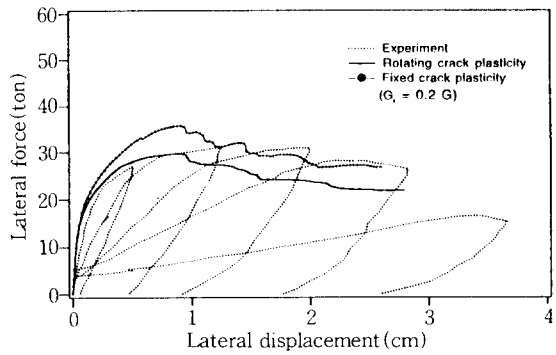

Fig. 8 Comparison between analyses and experiment for Wall 10

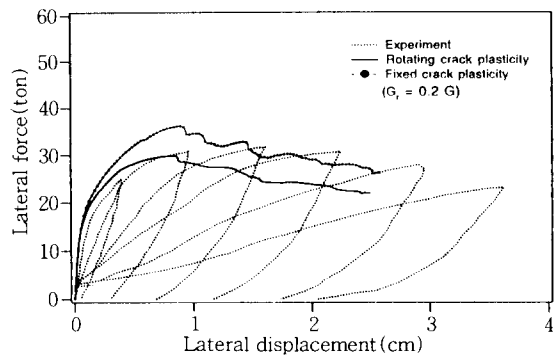

Fig. 9 Comparison between analyses and experiment for Wall 12

multiple failure criteria for crushing and cracking should be addressed simultaneously in the analysis of reinforced concrete members. This plasticity model using multiple failure criteria provides reasonable failure mode of reinforced concrete members in plane stress. According to idealization of crack orientations, rotating-crack and fixed-crack plasticity can be used for tensile behavior.

Analyses using the plasticity models show reasonable load-deflection curves which are consistent with the experiments of reinforced concrete member. The rotating-crack plasticity produce better agreement with the experiments than the fixed-crack plasticity. The fixed-crack plasticity overestimates the ultimate loads. This indicates that the tensile stress-strain relation in the idealized fixed crack direction does not accurately follows the rotation of principal axes due to the progressive cracking process of reinforced concrete.

In shear walls with fixed supports, the von Mises model does not produce good agreement with the post-crushing behavior. The Drucker-Prager model, which is more sensitive to confinement, should be used to consider confinement provided by the fixed supports.

The backward-Euler procedure used for integration of flow rule should be modified for multiple plasticity. Sometimes, the backward-Euler procedure does not accomplish convergence to failure surfaces with a reasonable number of iterations. This indicates that the given strain increments are too large for the integration. The given strain increments can then be divided into small steps, and each step is iterated. The steps are combined to give the stresses corresponding to the given strain increments.

Notations

$\underline{D}$=Elastic stiffness matrix

$\underline{D}_t$=Consistent tangent stiffness matrix

f_i=Failure criterion

G=Shear stiffness

G_r=Reduced shear stiffness

G_t=Fracture energy of tensile cracking

h=Effective length corresponding to Gauss point

$\underline{s}$=Deviatoric stress

δ_{ij}=Kronecker delta

$\dot{\lambda}_i$=Plastic strain rate multiplier

σ_e=Effective stress

$\bar{\sigma}_i$=Function of failure surface

$\Delta\underline{\sigma}$=Incremental stress vector

ε_{pi}=Equivalent plastic strain

ε_{syi}=Yield strain of reinforcing steel

$\Delta\underline{\varepsilon}$=Incremental strain vector

$\Delta\underline{\varepsilon}_e$=Incremental elastic strain vector

$\Delta\underline{\varepsilon}_p$=Incremental plastic strain vector

ρ_e=Effective reinforcement ratio

f_{xy}=Yield stress of reinforcing steel in x direction

ρ_x=Reinforcement ratio in x direction

ρ_y=Reinforcement ratio in y direction

References

1. ABQUS, "An Inelastic Constitutive Model for Concrete," *Theory Manual*, 1990.
2. Bresler, B. and Scordelis, A. C., "Shear Strength of Reinforced concrete Beams," *American Concrete Institute Journal, Proceedings*, Vol. 60, Jan. 1963, pp.51-72.
3. Crisfield, M. A., "Basic Plasticity," *Non-linear Finite element Analysis of Solids and Structures* Vol. 1, John Wiley & Sons Ltd., 1991.
4. Labbane, M., Saha, N. K., Ting, E. C., "Yield Criterion and Loading Function for concrete Plasticity," *Int. J. Solids Structures*, Vol. 30, No. 9, pp.1269-1288.

5. Feenstra, P. H., and de Borst, R., *Aspects of Robust Computational Modeling for Plain and Reinforced Concrete*, Heron, Vol. 4, 1993.
6. Park, H., Klingner, R. E., Wheat, D., "Numerical Techniques for Predicting Brittle Failure of Reinforced Concrete Planar Structures," *Journal of the Structural Division*, ASCE, Vol. 121, No. 10, pp.1507-1513, 1995.
7. Park H., "Nonlinear Finite Element Analysis of Reinforced Concrete Planar Structures," thesis presented to the University of Texas at Austin, in partial fulfillment of the requirements for the degree of Doctor of Philsophy, 1994.
8. Ramm, E. "Strategies for Tracing the Nonlinear Response Near Limit Points," Nonlinear Finite Element Analysis in Structural Mechanics, edited by Wundelich, W., Stein, E., and Bathe, K. J., Springer-Verlag, Berlin, 1981.
9. de la Rovere, H. L., "Nonlinear Analysis of Reinforced Concrete Masonry Walls under Simulated Serismic Loadings," thesis presented to the University of California at San Diego, in partial fulfillment of the requirements for the degree of Doctor of Philosophy, 1990.

(접수일자 : 1995. 8. 3)